Phys Chem Minerals (1997) 24: 206–221

ORIGINAL PAPER

S. Heinemann · T. G. Sharp · F. Seifert · D. C. Rubie

The cubic-tetragonal phase transition in the system majorite ($Mg_4Si_4O_{12}$) – pyrope ($Mg_3Al_2Si_3O_{12}$), and garnet symmetry in the Earth's transition zone

Received July 5, 1996 / Revised, accepted September 24, 1996

Abstract Garnets along the join $Mg_4Si_4O_{12}$ (majorite end member) – $Mg_3Al_2Si_3O_{12}$ (pyrope) synthesized at 2000 °C, 19 GPa are, after quench, tetragonal in the compositional range up to 20 mol% pyrope, but cubic at higher Al contents. Lattice constants a_{tet} and a_{tet} in the tetragonal compositional range converge with increasing pyrope contents towards the lattice constant of the cubic garnets. The elastic strain and the intensity of the (222) reflection as a function of composition indicate a second-order phase transition near 20 mol% pyrope. From the wedge-like shape of pseudomerohedral twins and their interaction near 90° twin-boundary corners, as well as from the absence of growth-induced dislocations, it is concluded that the Al-poor garnets are also cubic at synthesis conditions but invert by (Mg,Si) ordering on the octahedral sites into tetragonal phases of space group $I4_1/a$ upon quench. This implies that the cubic-to-tetragonal phase transition in $Mg_4Si_4O_{12}$ garnet occurs below 2000 °C at 19 GPa and at even lower temperatures in more aluminous compositions. A composition-dependent Landau model is consistent with a direct transformation from $Ia\bar{3}d$ to $I4_1/a$. Comparison of the *T*-*X* stability field of majorite-pyrope garnets with the chemistry of majorite-rich garnets expected to occur in the Earth's transition zone shows that the latter will be cubic under all conditions. Softening of elastic constants, which commonly accompanies ferroelastic phase transitions, may affect the seismic velocities of garnets in the deeper transition zone where majorite contents are highest.

S. Heinemann (✉) · T. G. Sharp[1] · F. Seifert · D. C. Rubie
Bayerisches Geoinstitut, Universität Bayreuth,
D-95440 Bayreuth, Germany

Present address:
[1] Nowat: Department of Geology, Arizona State University, Tempe, AZ 8528Z, USA

Introduction

Seismic discontinuities in the Earth's mantle are controlled by changes in the physical properties of the constituent mineral phases, which are a function of pressure, temperature, crystal structure and chemical composition. In detail, symmetry of the phases can also play an important role. For instance, a structural phase transition between tetragonal and orthorhombic $MgSiO_3$ perovskite may occur slightly below the 660 km discontinuity (Warren and Ackland 1996) and influence seismic velocity profiles.

It is generally agreed that garnets are dominant phases (in addition to β- and γ-$(Mg,Fe)_2SiO_4$) of the Earth's transition zone and that they are characterized by high concentrations of a majorite ($Mg_4Si_4O_{12}$) component (Weidner 1986, Ringwood 1991). These garnets, which can be approximated by the system majorite – pyrope ($Mg_3Al_2Si_3O_{12}$), will thus contribute significantly to the complex velocity structure of the transition zone.

Whereas pyrope appears to remain cubic at all *P*-*T* conditions of its stability field (e.g. Akaogi and Akimoto 1977), the $Mg_4Si_4O_{12}$ majorite end member has, at least after quench, tetragonal symmetry with a largely ordered Mg-Si distribution over two distinct octahedral sites (Angel et al. 1989; Phillips et al. 1992). This phase invariably exhibits both merohedral and pseudomerohedral twinning, which has been interpreted as evidence for a phase transition from cubic to tetragonal symmetry during the quench. Thus it has been inferred from the microtextures that under the conditions of synthesis (for example 17 GPa, 1800 °C) the majorite end member is actually cubic (Angel et al. 1989; Hatch and Ghose 1989), but the interpretation of microstructural evidence is not always clear-cut. Wang et al. (1993) concluded from the dependence of microstructures on the temperature of synthesis that the phase transition from cubic to tetragonal symmetry in the end member majorite occurs near 2350 °C at 22 GPa. This implies that the as-quenched tetragonal garnets synthesized below this

temperature actually grew as tetragonal garnets and that the ubiquitous twinning represents a growth feature. They concluded that majoritic garnets in the Earth's transition zone are likely to be tetragonal, a conclusion which has implications for their elastic properties and seismic wave velocities. An analogous phase transition in $Ca_3Mn_2Ge_3O_{12}$ garnet (Kazey et al. 1982) leads to a softening of the Youngs modulus by up to 15%, which implies that if a similar phase transformation occurs in transition-zone garnets, the effect on seismic velocities would be significant. Also, it is not clear whether the phase transition in majorite proceeds from the cubic $Ia\bar{3}d$ to the tetragonal $I4_1/a$ space group by a single step (with simultaneous formation of the merohedral and pseudomerohedral twins) or by two subsequent processes via an intermediate space group $I4_1/acd$.

The stability field of the majorite end member lies outside the reach of most *in-situ* measurements that could address the question of majorite symmetry at *P* and *T* directly. However, from the compositional dependency of the cubic to tetragonal phase transition in quenched phases of a solid solution series, we may also gain information on the order of the transition, its mechanism and the volume properties of the cubic vs. tetragonal phase, i.e. the compositional variation may be used as a substitute for temperature variation. Furthermore, physical properties (including symmetry) of majorite-pyrope solid solutions are more relevant to the transition zone than those of the pure majorite end member. In accordance with the original description of the majorite species (Smith and Mason 1970), we define majorites as garnet solid solutions with at least part of the octahedral site filled with Mg and Si independent of symmetry. The $Mg_4Si_4O_{12}$ garnet compound is then termed the majorite end member (Ma).

The central problems investigated in this study are therefore the symmetry of the majorite-pyrope solid solution garnets in their field of stability and after quench, the mechanism(s) of their phase transitions as a function of temperature and composition and the bearing of these findings on the symmetry of majoritic garnets in the Earth's transition zone.

Experimental methods

Synthesis

Garnet phases on the join $Mg_4Si_4O_{12}$ – $Mg_3Al_2Si_3O_{12}$ have been synthesized from glasses prepared from high-purity oxide mixes consisting of Al_2O_3 (>99.99%, Aldrich), MgO (99.95%, Johnson Matthey), and SiO_2 (99.995%, Aldrich), fused and homogenized at 1670 to 1750 °C. For $Mg_4Si_4O_{12}$ a crystalline mixture of proto- and clinoenstatite prepared by sintering oxides at 1500 °C for 24 hours was also used. Syntheses were performed at high temperature and pressure in a multianvil press using semi-sintered MgO (doped with 5% Cr_2O_3) octahedra of 10 mm edge length as the pressure medium and WC cubes with 32 mm edge length and 5 mm truncations. Details of the sample assembly are given by Canil (1994). Re capsules containing the starting material were in direct contact with the Re97%W3%-Re75%W25% thermocouple. Pressures have been calibrated against known phase equilibria (Canil 1994), and reported values are considered to be accurate within 1 GPa. Temperatures were controlled within ± 2 °C and are uncorrected for the effect of pressure on the emf of the thermocouple. Due to temperature gradients within the capsule, the temperature uncertainty is estimated to be ~ 80 °C at 2000 °C, based on the calibration by Canil (1994). Run durations varied from 2 to 15 min. Shutting off the power led to a temperature quench to below 300 °C within less than 2 s.

Electron microprobe analysis

Both starting glasses and synthesis products were analyzed using a CAMECA SX50 electron microprobe in wavelength dispersive mode with a beam diameter of 1–2 µm for crystals and 10–20 µm for glasses. Samples were coated with carbon and analyzed with 15 kV acceleration voltage and a 15 nA current. Spinel, forsterite, enstatite, orthoclase and pyrope (from Dora Maira) served as standards.

Powder X-ray diffraction

Product phases were identified using a Siemens D5000 diffractometer operating in reflection mode with Cu$K\alpha_{1,2}$ radiation. For the determination of precision lattice constants, a Stoe STADI P transmission diffractometer with Ge-monochromatized Co$K\alpha_1$ radiation and a position-sensitive detector (mini-PSD) was used. Samples were crushed at –196 °C because it had been shown by O'Neill et al. (1993) that structural damage to highly metastable phases during grinding can thus be avoided. Materials were then mixed with Si powder (NBS 640b) as an internal standard. Patterns were run from 11 to 139 degrees 2θ, with the 2θ scale corrected from the Si peak positions, and individual peaks were fitted to quadratic Lorentz functions. In the case of split peaks from tetragonal garnets, doublets or triplets were fitted with the constraint of equal half width. The pattern as a whole was fitted using Rietveld techniques only for the sample with the smallest tetragonal distortion. Peaks were indexed by comparison with a powder pattern calculated on the basis of the Angel et al. (1989) data for the majorite end member, and lattice constants were refined by least squares optimization with the LCLS routine (Prewitt, unpublished).

Transmission electron microscopy

The cylindrical capsules from the high-pressure experiments were cut along their long axes to make doubly polished thin sections of 30 µm thickness. The samples were mounted on 3 mm Pt grids and mechanically thinned to approximately 10 µm using a Gatan Dimple Grinder before being thinned by ion bombardment. Ion thinning was performed using a Gatan Duomill 600 with Ar ions (6 kV ions, 15° to the sample surface) until holes with electron-transparent rims were formed. Samples were coated with 5 to 10 nm of amorphous carbon to prevent charging in the electron microscope. Transmission electron microscopy (TEM) was performed using a 200 kV Philips CM20 FEG equipped with a super-twin objective lens and a Noran Voyager analytical system for energy dispersive X-ray analysis. Crystals were oriented for electron diffraction and imaging using a double-tilt sample holder with $\pm 25°$ of goniometer tilt.

Results

Synthesis and chemical composition

Syntheses at 19 GPa, 2000 °C led generally to single-phase garnet products. Table 1 lists the conditions and products of syntheses together with the chemical analyses of the garnet phases. Trace amounts of stishovite, observed only with TEM, occur as idiomorphic inclusions

Table 1 Results of syntheses

Run No.	Composition starting mat.	*P* (Gpa)	*T* (°C)	Duration (min)	Products (mol% pyrope)	Garnet composition	Remarks
H24	Ma100	18	2000	5	tet.Maj (Sti)		
881	Ma100	18	2000	3	tet.Maj (Cpx,Sti)	0.0	
H91	Ma100*	19	2000	10	tet.Maj (Cpx,Sti)	0.0	LCR
971	Ma100*	19	1900	3	tet.Maj (Cpx, Sti)	0.0	LCR
H221a	Ma100	19	2000	15	tet.Maj		TEM
H106	Ma96Py04	19	2000	11	tet.Maj		TEM
985	Ma96Py04	19	2000	7	tet.Maj (trace β)	3.58(58)	TEM
H95	Ma93Py07	19	2000	3	tet.Maj (trace Sti)		TEM
977	Ma93Py07	19	2000	3	tet.Maj	6.59(13)	LCR
H113	Ma91Py09	19	2000	3	tet.Maj (Sti)		TEM
833	Ma87Py13	19	2000	5	tet.Maj (Cpx)	12.85(77)	LCR
885	Ma87Py13	18	2000	2	tet.Maj (Cpx,Sti)	12.83(22)	
H127	Ma84Py16	19	2000	10	tet.Maj (trace Sti,β)	15.70(18)[§]	TEM
846	Ma81Py19	18	2000	5	tet.Maj (trace Sti)		
890	Ma81Py19	19	2000	5	tet.Maj (trace Sti)	19.06(81)	LCR
852	Ma74Py26	18	2000	5	cub.Maj (Cpx)		
882	Ma74Py26	19	2000	2	cub.Maj (Cpx,Sti)	25.92(81)	LCR
H125	Ma50Py50	19	2000	4	cub.Maj	50.19(57)	LCR
H221b	Ma50Py50	19	2000	15	cub.Maj		TEM
H124	Ma25Py75	19	2000	11	cub.Maj	75.12(40)	LCR
1000	Ma0Py100	19	2000	11	Pyrope	99.98(42)	LCR

The column composition gives the nominal composition of the starting material; glass or *pyroxene
Abbreviations: tet.Maj=tetragonal majorite, cub.Maj=cubic majorite, Py=pyrope, Sti=stishovite, Cpx=clinopyroxene, β=β-Mg_2SiO_4. ATEM=analytical transmission electron microscopy, LCR=used for lattice constant refinement, TEM=used for transmission electron microscopy, [§]=ATEM analysis, all others microprobe. Brackets are used to indicate minor amounts of accessory phases

in garnet, with a corresponding amount of β-Mg_2SiO_4 occurring outside the garnet grains. This might be due either to early nucleation of stishovite and incomplete resorption due to the formation of a garnet armour, or to the temperature gradients in the capsule. If the temperature was locally significantly lower than 2000 °C at 18–19 GPa, due to temperature gradients, stishovite + β-Mg_2SiO_4 could form locally as stable phases (Yusa et al. 1993).

Chemical analysis of the garnets by microprobe and analytical transmission electron microscopy (ATEM, Table 1) showed them to be homogeneous within the precision of the measurement (ca. 0.5 mol% pyrope) and close to that of the starting material. In particular, no systematic deviations from the theoretical 1:1 ratio of Mg:Si were observed throughout the series, confirming the substitution $(Mg^{2+}+Si^{4+})_{oct}\Psi 2Al^{3+}{}_{oct}$ in majorite.

Powder X-ray diffraction

Whereas garnets with up to ca. 13 mol% pyrope content clearly showed splitting of the relevant peaks into doublets or triplets due to tetragonal distortion, those with more than 20% pyrope content exhibited unsplit narrow lines. Figure 1 shows representative X-ray tracings of the cubic (400) peak that splits, in the tetragonal garnets, into the $(400)_{tet}$ and $(004)_{tet}$ peaks with a theoretical intensity ratio close to 2:1. The 19.06 mol% sample (run 890) had broadened peaks and was therefore refined as tetragonal, using the Rietveld technique. Lattice parameters thus refined were previously published (Heinemann et al. 1994) and are reported here in Table 2 and depicted in Fig. 2a.

Table 2 Lattice constants of garnets on the join majorite-pyrope

Run No.	pyrope (mol%)	α (Å)	*c* (Å)	*V* (Å^3)
H91	0.00	11.5187(3)	11.4204(4)	1515.258(51)
971	0.00	11.5186(4)	11.4200(7)	1515.183(88)
977	6.59	11.5093(19)	11.4422(33)	1515.669(419)
833	12.85	11.4961(16)	11.4582(26)	1514.330(309)
890	19.06	11.4798(12)	11.4751(24)	1512.063(426)
882	25.92	11.4755(2)		1511.167(24)
H125	49.85	11.4710(3)		1509.386(44)
H124	75.10	11.4644(4)		1506.802(47)
1000	99.98	11.4564(4)		1503.654(52)

The a_{cub} lattice constants of cubic garnets in the compositional range 20–100% pyrope, show a slightly nonlinear dependence on composition which can be expressed as

$$a_0[\text{Å}] = 11.4786(3) - 8.6(1.1)\cdot 10^{-5} X - 1.369(87)\cdot 10^{-6} X^2 \quad (1)$$

where X=mol% pyrope. The χ^2 test showed this nonlinearity to be significant (reduced $\chi^2_{nonlinear}=0.15$ vs. reduced $\chi^2_{linear}=18.56$). Similarly, dependence of volume on composition for the cubic garnets shows a small excess volume of mixing (Fig. 2b). Positive excess volumes due to mixing on the octahedral site have also been observed for garnets along the join $Ca_3Fe_2Si_3O_{12}$ – $Ca_3Sc_2Si_3O_{12}$ (Woodland, personal communication).

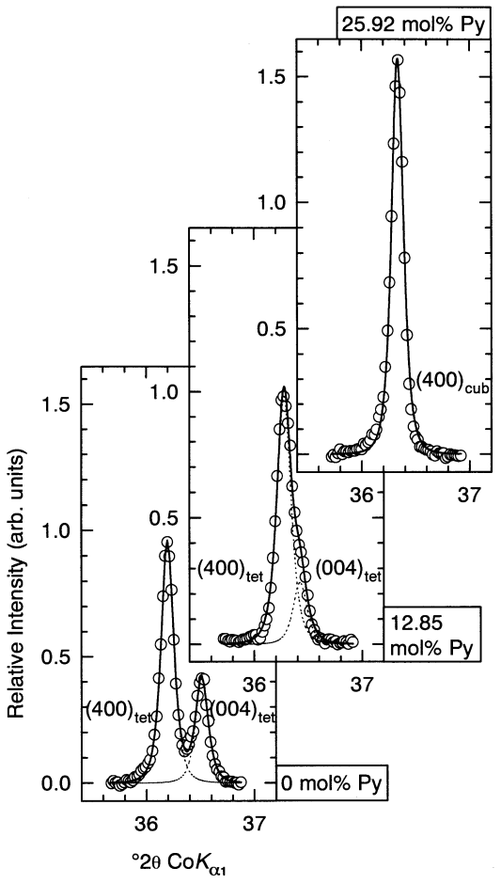

Fig. 1 (400) and (004) powder diffraction x-ray peaks of tetragonal and cubic majorites in the system $Mg_4Si_4O_{12}$-$Mg_3Al_2Si_3O_{12}$. The cubic (400) and tetragonal (400)-(004) doublets are fitted with a solid curve whereas the individual tetragonal (400) and (004) peaks are shown with dashed curves

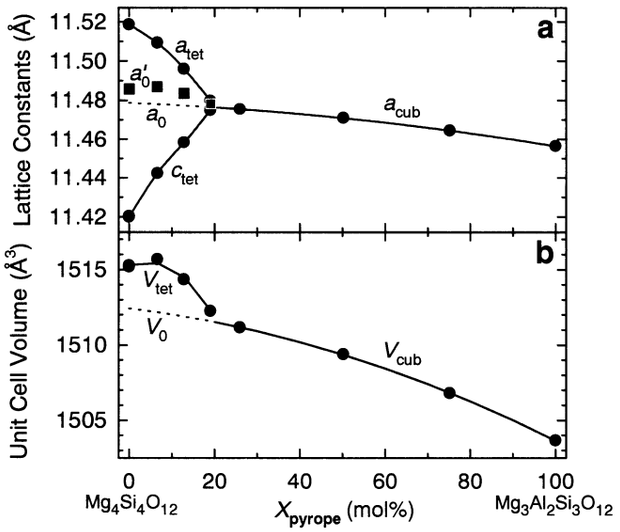

Fig. 2 **a** Lattice constants and **b** cell volumes of garnets in the system $Mg_4Si_4O_{12}$-$Mg_3Al_2Si_3O_{12}$. Also shown are the extrapolated cubic lattice constant a_0 and the calculated average cubic lattice constant a_0'

The increase in lattice constants from pyrope extrapolated towards a hypothetical cubic $Mg_4Si_4O_{12}$ majorite end member (Fig. 2) can be explained simply by comparing the ionic radii of cations involved in the substitution $2Al^{3+} \Psi Mg^{2+} + Si^{4+}$. The average octahedral radius increases from 0.53 Å for Al to 0.56 Å for (Mg+Si)/2 (effective ionic radii taken from Shannon 1976).

For tetragonal garnets, in the compositional range 0–20% pyrope, a_{tet} is larger than c_{tet}, with a_{tet} steeply increasing and c_{tet} decreasing with increasing majorite contents, i.e. an increase in the tetragonal distortion occurs with decreasing pyrope content. A characteristic feature of the lattice constants and volumes as a function of composition is that the tetragonal and cubic values converge at a point close to 20 mol% pyrope. Defining an average cubic lattice constant in the tetragonal range such that $a_0' = (2a_{tet} + c_{tet})/3$ (Fig. 2a) it can be seen that the extrapolated cubic lattice constant a_0 is smaller than a_0', and that tetragonal volumes are higher than the extrapolated cubic ones, which indicates that the transition is improper ferroelastic.

The relative deformation of the unit cell metrics at this phase transition may be expressed (Salje 1990) by the total spontaneous strain e^{tot}:

$$e_{11}^{tot} = (a_{tet} - a_0)/a_0 \quad (2)$$

$$e_{33}^{tot} = (c_{tet} - a_0)/a_0 \quad (3)$$

The proper ferroelastic strain e^{elas} is defined as (Aizu 1969, Salje 1990)

$$e_{11}^{elas} = 1/3\,(a_{tet} - c_{tet})/a_0 \quad (4)$$

$$e_{33}^{elas} = -2e_{11}^{elas} \quad (5)$$

Both e_{11}^{tot} and e_{11}^{elas} increase towards $Mg_4Si_4O_{12}$, whereas the difference between e^{tot} and e^{elas} (the additional, non-symmetry-breaking, non-volume conserving strain e^{add}) levels off at about 7 mol% pyrope (Fig. 3a). From the ferroelastic deformation as a function of composition X, the critical composition X_c for the phase transition and the order parameter exponent β can be calculated (Landau and Lifschitz 1980):

$$e_{11}^{elas} = b\,(X_c - X)^{2\beta} \quad (6)$$

where b=scaling factor. Fitting of experimental strain values (Fig. 3a) yields $b = 1.78(12) \cdot 10^{-4}$, $\beta = 0.46(1)$ and $X_c = 19.88(15)$ mol% pyrope. As discussed later, the order parameter exponent β is very close to the theoretical value of 0.5 for an ideal continuous phase transition of second order.

The intensity of the (222) peak as a function of pyrope content provides further insight into the phase transition, as it is symmetry-forbidden in the cubic $Ia\bar{3}d$ space group (as well as in the tetragonal space group $I4_1/acd$ to be discussed later), but allowed in the tetragonal space group $I4_1/a$, which is that of the pure $Mg_4Si_4O_{12}$ end

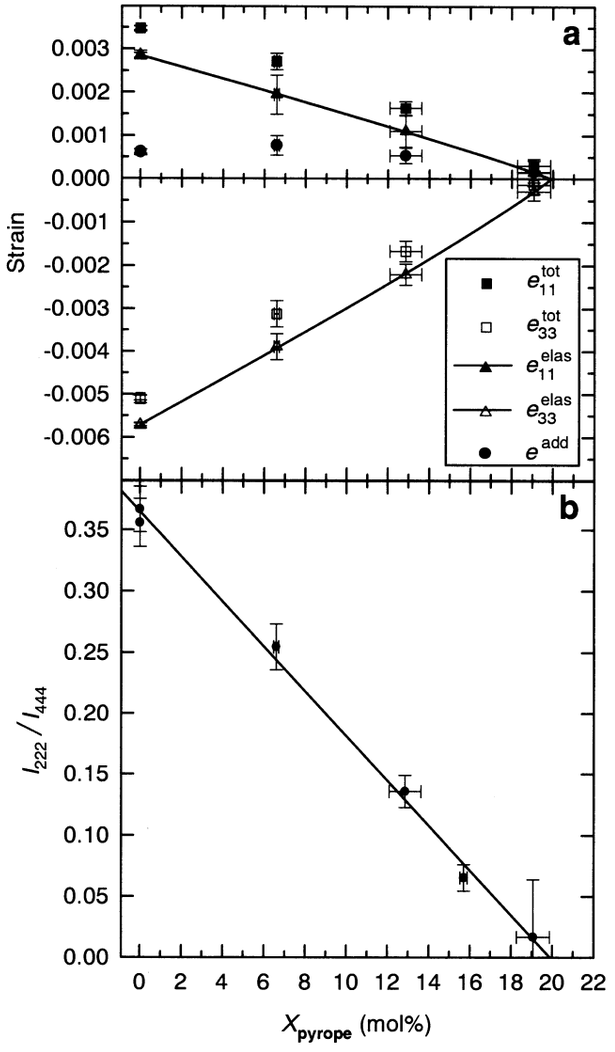

Fig. 3 **a** Total, elastic and additional strain ($e_{11}{}^{tot}$, $e_{33}{}^{tot}$, $e_{11}{}^{elas}$, $e_{33}{}^{elas}$, e^{add}) in tetragonal majorite garnets as a function of composition, calculated from their lattice constants and those of extrapolated cubic garnets. The curves represent a fit to the ferroelastic strain $e_{11}{}^{elas}=-2\ e_{33}{}^{elas}\propto|X_c-X|^{2\beta}$ with $\beta=0.46$. The convergence of all strains to zero defines the critical composition X_c for the phase transition. **b** Integrated normalized intensity of the (222) peak in tetragonal majorite garnets as a function of composition. The straight line ($I_{222}\propto|X_c-X|$) defines a second order phase transition with a critical composition close to 20 mol% pyrope

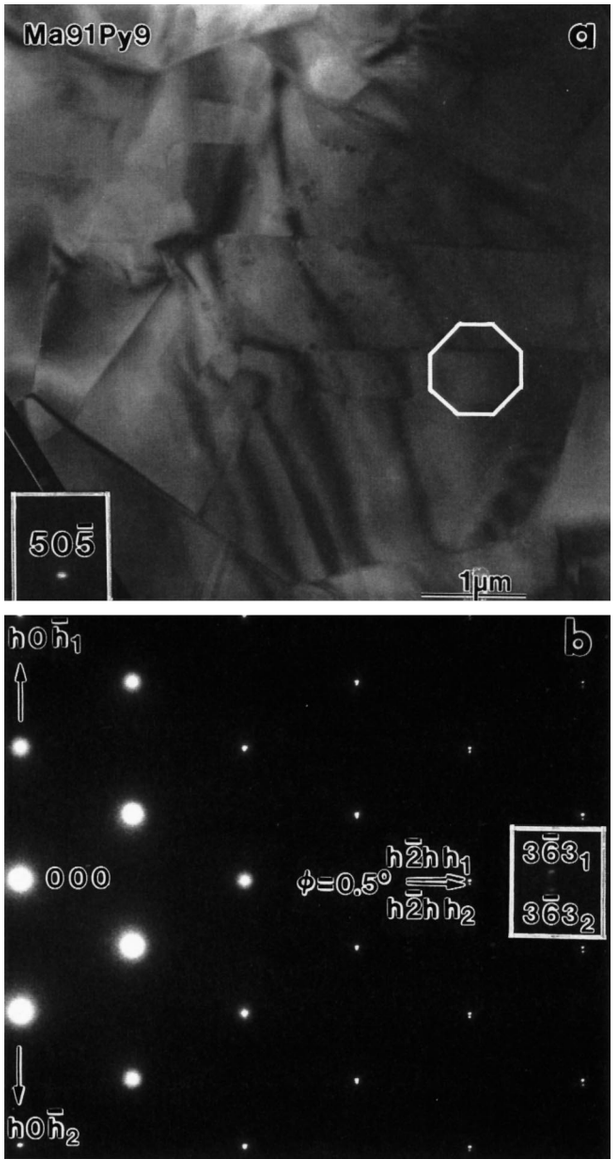

Fig. 4 **a** Bright-field image of pseudomerohedral twins in $Ma_{91}Py_9$ garnet. The crystal was slightly inclined from the [111] zone axis for better contrast of the twins. **b** One half of the [111] zone-axis diffraction pattern from the region marked in (a) shows splitting along $[10\bar{1}]^*$ of reflections outside of the (*h*0*h*) row. The degree of splitting is represented by the angle $\phi=0.5°$ between split reflections perpendicular to $[10\bar{1}]^*$. The split $(3\bar{6}3)$ and unsplit $(50\bar{5})$ reflections are enlarged to illustrate splitting outside the (*h*0*h*) row.

member (Angel et al. 1989). The observed (222) peak intensities, normalized to those of (444) which is allowed in all space groups to be considered, can be fitted with a straight line (Fig. 3b). As from the consideration of elastic strain, the critical composition is found to be close to 20 mol% pyrope (Fig. 3), but the intensity of the (222) peak in the 19.29 mol% pyrope sample is too small and uncertain to make definite statements about the transition region itself.

Transmission electron microscopy

The change in symmetry along the solid solution series is reflected in TEM data by systematic extinctions in the SAED patterns (combined with information from the X-ray powder diffraction patterns) and by the changes in microtextures, particularly the existence of twinning in

the tetragonal garnets and its absence in the cubic phases. Investigated run products are listed in Table 1.

Whereas the extinction symbol of the $Ma_{50}Py_{50}$ garnet is *Ia_d*, proving the cubic space group $Ia\bar{3}d$, that of all garnets with less than 20 mol% pyrope is *I_/a_ _*, i.e. the *d* glide plane in $Ia\bar{3}d$ is lost. From the existence of merohedral twins in these phases (see below), the Laue class is $4/m$, which, combined with the extinction symbol, is consistent with the tetragonal space group $I4_1/a$.

All tetragonal majorites contain merohedral and pseudomerohedral twins as observed for the pure majorite end member by Angel et al. (1989). Mirror planes for the pseudomerohedral twins are the cubic (101), $(10\bar{1})$, (011), and $(01\bar{1})$ planes ($\{101\}_{tetragonal}$), whereas for merohedral twins they are the cubic (110) and $(1\bar{1}0)$ planes ($\{110\}_{tetragonal}$). Again, this is consistent with space group $I4_1/a$ because the cubic mirror planes relating the twins are not mirror planes in this tetragonal space group. The exchange of the unequal a and c axes by pseudomerohedral twins causes strain in the crystal and splitting of reflections in electron diffraction patterns (Salje 1990, Nord 1992). An example of pseudomerohedral twins, for the 9%-pyrope composition, is shown in Fig. 4 with the corresponding splitting of diffraction peaks due to the reflection across the twin of reciprocal lattices that are slightly inclined relative to the twin plane. The angle ϕ between the split reflections is 0.5°, which corresponds to the strain measured by X-ray diffraction for this composition. Merohedral twins, in contrast to the pseudomerohedral twins, result in the superposition of equal lattice parameters and do not result in ferroelastic lattice strain. The twin boundaries are therefore not constrained to planes of minimum strain and tend to be curved and irregular (Fig. 5).

There seems to be some confusion about merohedral twins and antiphase boundaries in such materials. Order-

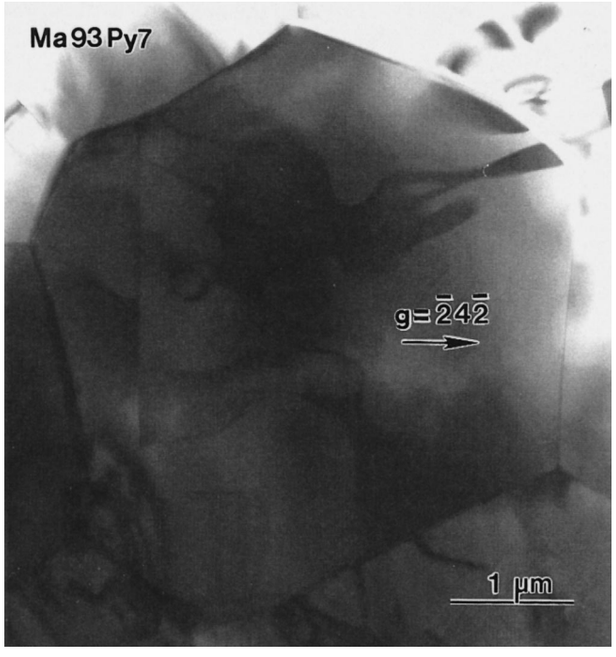

Fig. 5 Merohedral twins in $Ma_{93}Py_7$ garnet. The bright-field image, with the $(\bar{2}4\bar{2})$ reflection excited, shows rounded and curved twin domains. Domain contrast is produced by the difference in structural amplitudes of the superimposed $(\bar{2}4\bar{2})$ and $(4\bar{2}\bar{2})$ reflections of the twin individuals

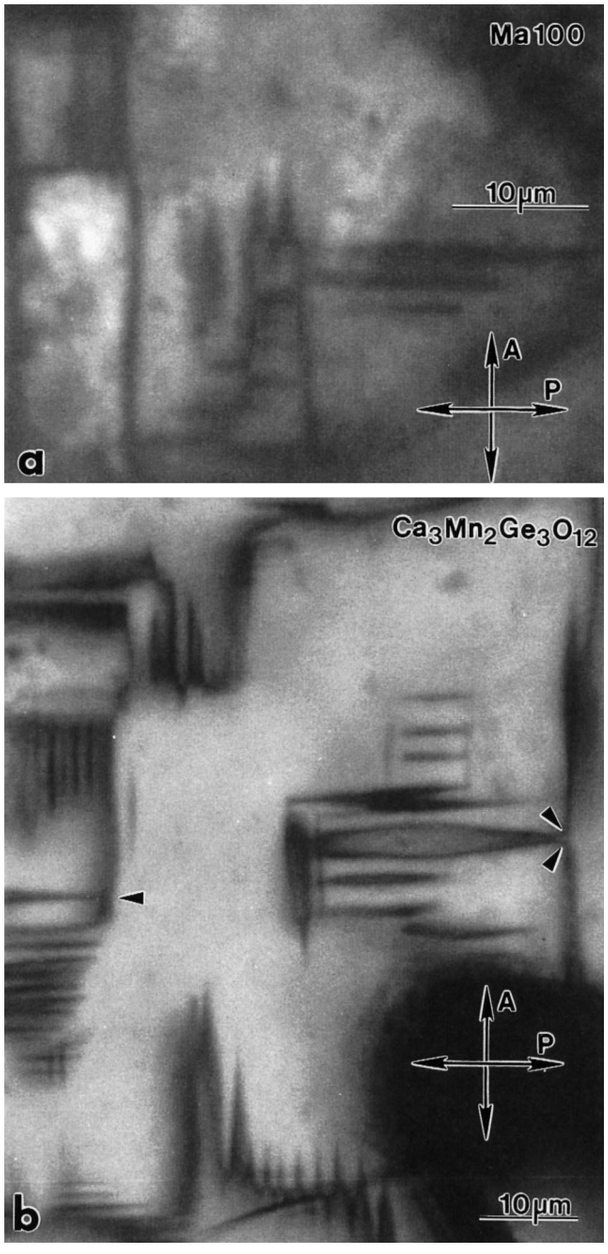

Fig. 6a, b Optical micrographs of needle-form pseudomerohedral twins in **a** the majorite end member and **b** in $Ca_3Mn_2Ge_3O_{12}$ garnet obtained with crossed nicols (the analyser A and polariser P directions are parallel to the twin domains). Domain walls are visible through deformation contrast. *Arrows* (**b**) indicate interactions between 90° domain-wall corners which leads to the formation of needles

ing of Mg and Si cations of the majorite end-member is inverted at the merohedral twin boundaries, such that if one considers the sublattice of octahedral cations only, merohedral twins have an antiphase character. On the other hand, the contrast of merohedral twins is distinct from that of anti-phase boundaries because merohedral twins can show domain contrast, whereas anti-phase boundaries only show boundary contrast. Contrast is observed for merohedral twins only for reflections (*hkl*) with $h \neq k$ where there is a difference in structure factor. For the symmetry-equivalent reflections (*hhl*), (*h*0*l*)⇔(0*kl*) and (*h*00)⇔(0*k*0), no merohedral contrasts are observed.

Pseudomerohedral twins, which often exhibit a characteristic needle-like shape (actually wedge-like in three dimensions, cf. Yamamoto et al. 1977a, b), are coarse enough in the majorite end member to be seen in the petrographic microscope (Fig. 6a). These textures are identical to those observed in $Ca_3Mn_2Ge_3O_{12}$ garnet (Fig. 6 this study, Gnatchenko et al. 1986), which undergoes a ferroelastic phase transition from $Ia\bar{3}d$ to a tetragonal phase described in space group $I4_1/a$ by Gnatchenko et al. (1986) upon cooling below 230 °C (Fig. 6b). The needles in ferroelastic crystals originate from the merger of 90° twin boundary junctions which have high elastic strains, and result in the needle-shaped twins (Fig. 6b) with much lower elastic strain pointing in the direction of a perpendicular twin wall (e.g. Salje et al. 1985; Palmer et al. 1988). The same features are observed in TEM in the Al-bearing tetragonal majorites, but on a finer scale (Fig. 7). Because the pseudomerohedral twins observed in the majorite garnets all have this needle-twin microstructure characteristic of ferroelastic phase transitions, we interpret the twins to be a result of the phase transition rather than a result of growth or deformation. This important conclusion will be discussed in greater detail below.

The nature of the twinning in the $Ma_{84}Py_{16}$ garnet deserves an additional comment. This composition is closest to the critical pyrope content (20% pyrope), i.e. it has the smallest tetragonal deformation, and both the pseudomerohedral and merohedral twins show peculiarities. Merohedral twin domains are only ~10 nm in diameter and are smaller than those in the less aluminous majorites by a factor of ~100 (Fig. 5). Pseudomerohedral twins occur in two types of grains: *i*) As coarse domains near the edge of grains but not in their centre (Fig. 8). The diagnostic reflections for tetragonal majorite (0 2*k*+1 2*l*+1) are strong at the rim but virtually

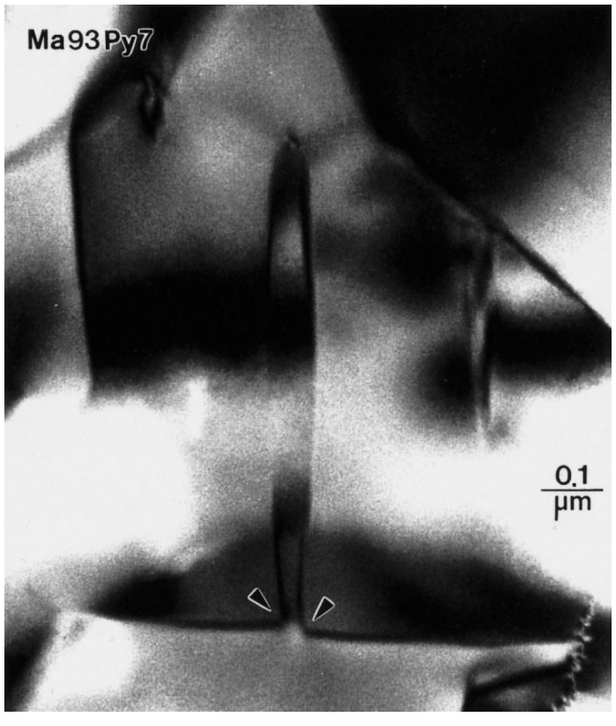

Fig. 7 Needle-like pseudomerohedral twins in $Ma_{93}Py_7$ garnet showing interaction of domain walls near 90° corners (*arrows*). Merger of such 90° corners produces the sharp needle like twins

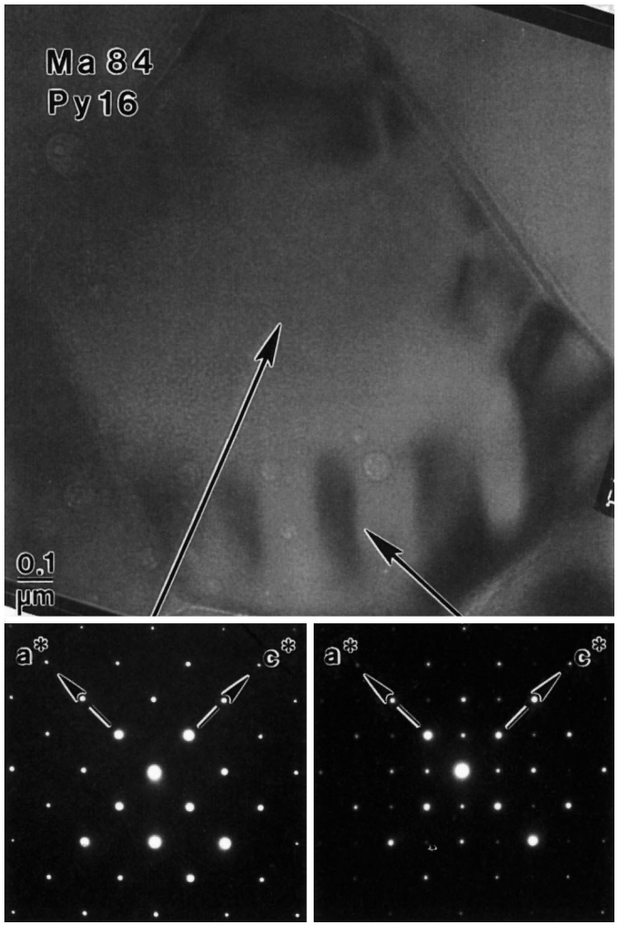

Fig. 8 Grain of $Ma_{84}Py_{16}$ garnet showing fairly coarse pseudomerohedral twins near the grain boundary, where strong tetragonal (0 2*k*+1 2*l*+1) reflections are observed in SAED patterns (*bottom right*). In the grain centre the critical (0 2*k*+1 2*l*+1) reflections are extremely weak (*bottom left*) and twins are not visible.

absent in the core, indicating close to cubic symmetry in the core and tetragonal symmetry at the rims. The twin domains at the rims of these grains appear to be pseudomerohedral twins, but without the sharp boundaries or needle-like shapes that we see for such twins in more majorite-rich compositions. Such diffuse boundaries may be a result of less stringent control of domain boundary orientations because of the small lattice strain expected for this composition. These features suggest that either the transformation from cubic to tetragonal started at the grain boundary, but did not reach the centre of the grain, or that grains may be compositionally zoned such that cores are slightly more pyrope-rich than rims. *ii*) Other grains have a very fine-grained (nm scale) pseudomerohedral tweed, which can be seen in dark-field images obtained with $\mathbf{g}=(044)$ and $\mathbf{g}=(0\bar{4}4)$ (Fig. 9) as streaks parallel to the diffraction vectors used. The lattice strain expected for these reflections is perpendicular

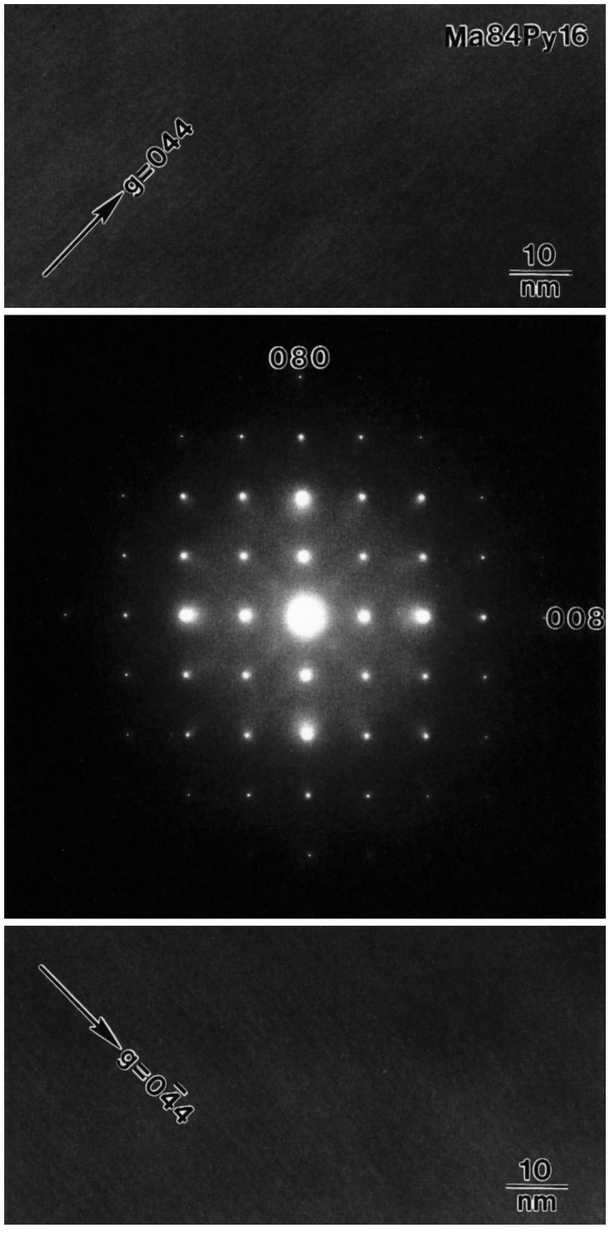

Fig. 9 Fine-grained pseudomerohedral tweed in $Ma_{84}Py_{16}$ majorite garnet is observed as nanometre-scale streaks in dark-field images obtained with diffraction vectors $\mathbf{g}=(044)$ and $\mathbf{g}=(0\bar{4}4)$. In the diffraction pattern, diffuse and weak diagnostic reflections $(0\ 2k+1\ 2l+1)$ can be seen as well as a disc of diffuse scattering intensity around the zero peak with a radius of [400]*. In the first and third quadrant diffuse streaks are observed parallel to [011]*, and parallel to $[0\bar{1}1]$* in the second and fourth quadrant. They extend from the peaks towards the zero point

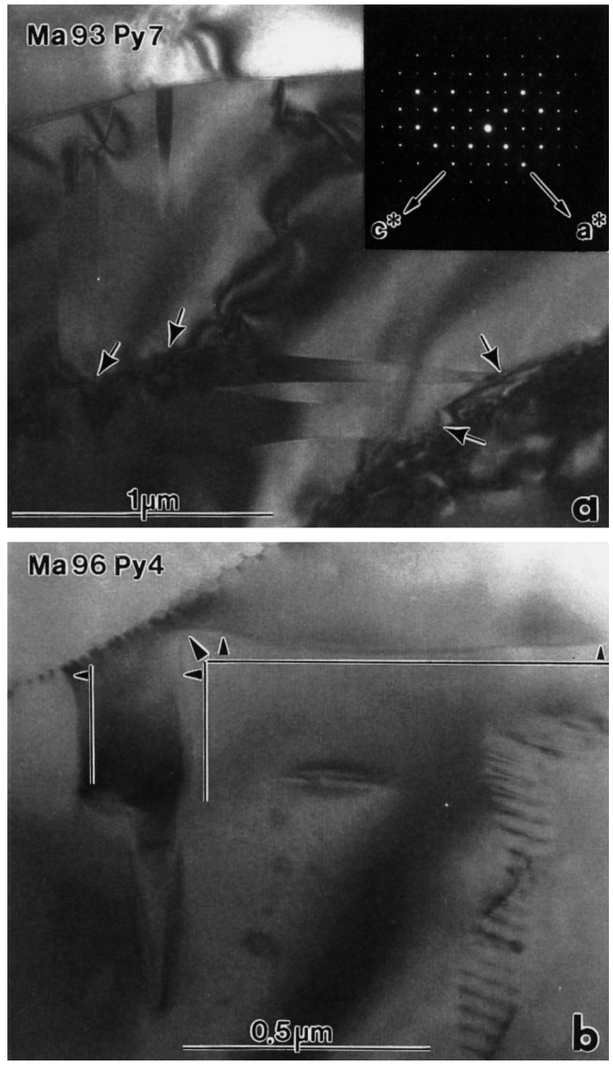

Fig. 10 **a** Pseudomerohedral twins in $Ma_{93}Py_{7}$ garnet terminating at dislocation walls (*arrows*). The dislocation wall in the centre of the image consists of few dislocations, indicating that very few are needed to pin twin boundaries. The [100]-zone diffraction pattern shows that the needles are parallel to {101} planes. **b** The presence of dislocation walls (*upper left*) causes distortion of a rectangular pseudomerohedral domain wall corner through the interaction of their strain fields. The distortion of the twin boundaries relative to the ideal shape (*straight lines*) is indicated by *arrows*

to the diffraction vectors and therefore results in streaking parallel to the diffraction vector in the images. The low magnitude of strain in this composition makes the nanometer-scale tweed difficult to image, being only visible in dark-field images with very high magnifications. In SAED patterns from this material, weak and diffuse critical (0 $2k+1$ $2l+1$) reflections as well as a central disk of diffuse scattering are visible (Fig. 9).

All synthesized garnets show distinct dislocation microstructures. In the cubic and tetragonal garnets both free dislocations as well as dislocation networks forming "dislocation walls" are observed. In the tetragonal majorite garnets, free dislocations and dislocation walls interact with the pseudomerohedral twin boundaries. Needle-like pseudomerohedral twins often start (or end) at such dislocation walls, bur never transect them (Fig. 10a). Because twins cannot simply terminate within the crystal without twin boundaries, pseudomerohedral twin boundaries must follow dislocation walls at such terminations (Figs. 10a, b). Likewise, 90° corners and boundaries of pseudomerohedral twins are deformed in the vicinity of dislocation walls as a result of interacting strain fields of both types of defects (Fig. 10b). Similar deformation of twin boundaries near other twin boundaries are described by Salje (1990). On the other hand, the dislocation walls themselves do not terminate or deform in the vicinity of domain walls. From these observations we conclude that the dislocation walls originated prior to the formation of the pseudomerohedral twins, which is consistent with the pseudomerohedral twins forming during quench.

Discussion

The composition-dependent phase transition

The continuous convergence of the tetragonal lattice constants towards the cubic lattice constant (Fig. 2a) is caused by the change in pyrope concentration. The critical pyrope concentration X_c=20%, as derived above from the strain considerations and the intensity changes in the (222) reflection, marks the transition from tetragonal to cubic symmetry in the as-quenched samples. All experimental observations (intensity of the (222) reflection, Fig. 3b; the continuous evolution of elastic strain, Fig. 3a; the systematic extinctions; the presence of both pseudomerohedral and merohedral twins in all tetragonal garnets) indicate that the transition from low- to high-alumina garnets is from space group $I4_1/a$ to $Ia\bar{3}d$, i.e. from an ordered octahedral arrangement of Mg on the octahedral site to a disordered one (McMillan et al. 1989). However, at this stage in the discussion we cannot entirely exclude the existence of a narrow compositional region close to the phase transition with the intermediate tetragonal space group $I4_1/acd$ (see below).

We would expect, in the field of tetragonal garnets, a systematic change of microtextures as a function of pyrope concentration because the driving forces (as described by the elastic strain shown in Fig. 3a) change with composition. For instance, Schmahl et al. (1989) as well as Krekels et al. (1990) report for Co- and Fe-doped $YBa_2Cu_3O_{7-x}$ a decrease in the spacing of transformational ferroelastic domain walls with increasing level of doping and consequent decrease of ferroelastic deformation. In general, we see such a trend, from the optically visible twinning in the majorite end member (Fig. 6a) via the sub-μm twin sizes in intermediate compositions $Ma_{97}Py_3$ to $Ma_{91}Py_9$ (Figs. 4, 5, 7, 10) to twins on a scale of a few nm ($Ma_{84}Py_{16}$ composition, Fig. 9). However, in the intermediate compositional range, sizes of domains vary between individual grains of a single sample, or even between subgrains. This cannot be due to chemical heterogeneities of the samples, as the scatter in the microprobe analyses was always less than 1 mol% pyrope concentration (Table 1). On the other hand, it has been shown above that the pseudomerohedral twins formed after the dislocation walls, where the locations of twin boundaries, and probably the sizes of the twins are influenced by the strain associated with dislocation walls.

The strong diffuse scattering of electrons from the $Ma_{84}Py_{16}$ sample (Fig. 9), which is close to the critical composition, is most likely related to short-range order effects and not to the lattice deformation accompanying the tweed. Although simulations would be required to interpret the diffuse scattering in terms of the ordering scale, we tentatively conclude that in this sample no perfect long-range order of octahedral cation distribution exists as would be characteristic for garnets in space group $I4_1/a$.

The fine-scale twinning and diffraction effects in the $Ma_{84}Py_{16}$ sample are somewhat different from the tweed features observed by Wang et al. (1993) in end-member majorite quenched from 2500 °C. The tweeds seen by Wang et al. (1993) should be more easily imaged than those in our $Ma_{84}Py_{16}$ sample because of the larger lattice strain in the end member composition. The larger strain should be clearly visible as streaking in the SAED patterns, but the interpretation of their streaks (Fig. 5b of Wang et al. 1993) is unclear. Streaking or splitting from a pseudomerohedral tweed should occur only along the $\langle 101\rangle^*_{\text{tetragonal}}$ directions, forming star-like reflections in electron diffraction patterns in $\langle 111\rangle$ zone axes (e.g. Heaney and Veblen 1990). The streaking shown by Wang et al. (1993) is not constrained to the $\langle 101\rangle^*_{\text{tetragonal}}$ directions and appears to be concentric about (000), suggesting that it represents slight misorientations from a subgrain microstructure. Furthermore, a pseudomerohedral tweed viewed along [111] should have three modulations forming 60 degree angles, but those shown (Fig. 5a of Wang et al. 1993) appear to be perpendicular. In our $Ma_{84}Py_{16}$ samples streaking is absent because the lattice strain is simply too small to resolve by electron diffraction. The small lattice strain leads to very little strain contrast when imaging tweeds in the $Ma_{84}Py_{16}$ sample.

The temperature-dependent phase transition

By comparison with the microtextures in $Ca_3Mn_2Ge_3O_{12}$ garnet (Fig. 6) it has been concluded above that the pseudomerohedral twins in the tetragonal majorite garnets are the product of a phase transition during isobaric temperature quench and that they cannot be growth twins. This comparison is legitimate although the cause of the transformation is different in the two cases. In the $Ca_3Mn_2Ge_3O_{12}$ garnet the transformation is due to a Jahn-Teller distortion of the Mn^{3+} in octahedral sites, whereas in the majorite garnets the transformation is connected with octahedral (Mg, Si) ordering. In both cases, however, atomic displacements are small, the connectivity of the polyhedra remains unchanged, and transformation involves the same space groups. The tetragonal deformation of the lattice and the consequent twinning in the two garnets are thus independent of the structural cause, and their transitions are symmetry-equivalent because the symmetry changes are identical.

A further argument in support of transformation twins as opposed to growth twins can be constructed from symmetry considerations and the orientations of the domain walls. The symmetry reduction during transformation leads to n different orientations of domains of the low-symmetry phase, where

$$n=|G|/|H|\cdot Z_H/Z_G \tag{7}$$

with $|G|$, $|H|$=order of the point groups describing the symmetry of the lattices G and H, and $Z_{G,H}$=number of formula units in the primitive unit cells of G and H (van Tendeloo and Amelinckx 1974; Janovec 1974). In the case of the transformation considered here, n=6. Three of these six orientations are ferroelastic with their tetragonal lattice deformation being described by the tensors

$$\mathbf{S}_{ij}^{S_1}=\begin{pmatrix} e_{11} & 0 & 0 \\ 0 & e_{11} & 0 \\ 0 & 0 & -2e_{11} \end{pmatrix} \quad \mathbf{S}_{ij}^{S_2}=\begin{pmatrix} e_{11} & 0 & 0 \\ 0 & -2e_{11} & 0 \\ 0 & 0 & e_{11} \end{pmatrix}$$

$$\mathbf{S}_{ij}^{S_3}=\begin{pmatrix} -2e_{11} & 0 & 0 \\ 0 & e_{11} & 0 \\ 0 & 0 & e_{11} \end{pmatrix} \tag{8}$$

The constraint for the orientation of domain walls between these follow (Sapriel 1978) from the conditions that the transition-induced change in length of common lattice vectors of both domains must be equal, i.e.

$$(\mathbf{S}_{ij}^{S_n}-\mathbf{S}_{ij}^{S_m})\,x_i x_j=0 \tag{9}$$

$$\text{ó}\ \det(\mathbf{S}_{ij}^{S_n}-\mathbf{S}_{ij}^{S_m})=0 \tag{10}$$

$$\text{ó}\ \mathrm{tr}(\mathbf{S}_{ij}^{S_n}-\mathbf{S}_{ij}^{S_m})=0 \tag{11}$$

$$\text{ó}\ (1\bar{1}0)_{cub},\ (011)_{cub},\ (101)_{cub},\ (1\bar{1}0)_{cub},\ (01\bar{1})_{cub},\ (10\bar{1})_{cub}=\underline{\underline{\{101\}_{tet}}}$$

Therefore, walls between twin domains can only occur parallel to $\{101\}_{tet}$, corresponding to the observed orientations which produce equal displacements of atoms on the joint structural planes. This could still be a growth phenomenon, but the decisive difference between growth-induced and transition-induced domains are in the 90° corners of the domain walls. Although such corners may occur in growth twins, they must be present in transformation twins, because $(101)\perp(101)$ and $(011)\perp(01\bar{1})$. In growth twins, the highly strained 90° corners would require dislocations to accommodate the misfit between adjacent domains and take up the strain. Such dislocations would decrease the mobility of 90° corners and hinder their merger into needle-shaped (actually wedge-like) domains. In the case of transformation-induced twinning, such misfit dislocations would not form, but instead all of the stress at the corners would be accommodated by elastic strain, leading upon relaxation and interaction with opposing 90° domain walls to the formation of needle-shaped domains (Yamamoto et al. 1977a, b; Salje et al. 1985). The absence of dislocations at domain corners and the interaction of domain corners to produce needles is considered stringent evidence for the origin of the pseudomerohedral twins through transformation.

In summary, all microtextural observations show that the garnets, which now are tetragonal after quench, were cubic under the conditions of synthesis, indicating that the phase transition must occur at a temperature below 2000 °C at a pressure of 19 GPa. On the basis of microtextural observations alone it cannot be determined whether this phase transition occurred in a single step, from $Ia\bar{3}d$ to $I4_1/a$ directly with the merohedral and pseudomerohedral twins forming simultaneously, or via a $I4_1/acd$ intermediate space group (with pseudomerohedral twins) leading to an ordered structure with a $I4_1/a$ space group and merohedral twins in a second step. We will return to this point later.

The overall conclusions for the origin of twinning and the existence of a phase transition are similar to those of Angel et al. (1989) for the majorite end member synthesized at 17 GPa and 1800 °C. On the other hand, Wang et al. (1993) grew $Mg_4Si_4O_{12}$ majorite at 2050 °C, 21.9 GPa from a $PbO+PbF_2$ flux and concluded from the size of the pseudomerohedral twins that they must be growth features. Majorite synthesized at 22.4 GPa, 2430 °C without flux also showed pseudomerohedral twins at the cold end of the capsule but a fine-scale modulation (tweed) at the hot end, whereas a synthesis without flux at 22.6 GPa, 2500 °C only showed a fine-scale modulation, which was interpreted as evidence for the onset of the cubic to tetragonal phase transition upon quench. From these observations Wang et al. (1993) concluded that the phase transition occurs at the temperature where the tweed structure passes into that of the pseudomerohedral twin, i.e. near 2350 °C at 22 GPa. However, the assumption that coarse twins must be growth twins is not cogent, because coarse transformational twins are the rule rather than the exception, e.g. in superconductors (Schmahl et al. 1989; Krekels 1990) as well as in the $Ca_3Mn_2Ge_3O_{12}$ garnets. The transformation twins observed here in Al-poor phases have similar dimensions to

those of the majorite end member of Wang et al. (1993) quenched from 2050 °C. Those of our $Ma_{84}Py_{16}$ sample are similar to the $Mg_4Si_4O_{12}$ garnets of Wang et al. (1993) quenched from 2430 and 2500 °C. Size alone is not a strong argument in this context, especially if flux-grown and unfluxed samples are compared. Therefore the conclusion that twinned garnet grew at 21.9 GPa, 2050 °C within the stability field of a tetragonal phase is open to doubt.

Landau Model of the phase transitions

According to Landau (1937a, b) the change in Gibbs Free energy across a phase transition may be described by a power series of an order parameter Q which transforms according to the active representation of the transition. For the improper ferroelastic path $Ia\bar{3}d \rightarrow I4_1/a$, with irreducible representation T_{1g}, we obtain for a second order phase transition

$$\Delta G_{T1g} = 1/2\, p(T-T_c)Q^2_{T1g} + 1/4\, qQ^4_{T1g} + 1/2\, rPQ^2_{T1g} + sXQ^2_{T1g} + t\varepsilon Q^2_{T1g} + u\varepsilon^2 \quad (12)$$

ΔG_{T1g} only contains even exponents of Q_{T1g}. The term $1/2\, rPQ^2_{T1g}$ describes the contribution of pressure (and volume, because r is in units of volume) to the change in free enthalpy, and $t\varepsilon Q^2_{T1g}$ reflects the contribution of the total tetragonal deformation (ε). It couples linearly quadratic with Q_{T1g} because T_{1g}: [yy–zz][yz] is not proportional to a deformation tensor of rank 2, but its product $T_{1g} \otimes T_{1g} = E_g + A_{1g}$ is proportional to the ferroelastic strain (E_g) and the volume change (A_{1g}) (where "⊗" indicates a symmetrised product representation and "+" relates to the sum of irreducible representations, Palmer et al. 1990). The term $u\varepsilon^2$ is the elastic energy contribution to the excess free energy. Term sXQ^2_{T1g} represents the contribution to enthalpy by the change in composition (X/100=mole fraction [Py]/([Ma]+[Py])). Following Salje et al. (1991) the coupling between X and Q_{T1g} is linearly quadratic:

$$\Delta G^{Ma-Py} = \Delta G^{Ma} + sXQ^2_{T1g} \quad (13)$$

From the condition of elastic equilibrium $\delta(\Delta G)/\delta\varepsilon = 0$ the relationship between deformation and the order parameters is obtained:

$$\delta(\Delta G)/\delta\varepsilon = 0 \quad (14)$$

$$\varepsilon = -1/2\, t/u\, Q^2_{T1g} \quad (15)$$

Substitution into the polynomial for ΔG yields the renormalized critical temperature T_c* for the transition:

$$T^*_c = T_c - (r/p)P - 2(s/p)X \quad (16)$$

Whereas the behaviour of the order parameters Q is generally described by $Q \propto |T_c - T|^\beta$ we here keep pressure and temperature constant but change X. If the coupling constants of deformation are independent of composition, the following relation for the total strain (ε) is obtained:

$$Q_{T1g} \propto |X_c - X|^\beta \quad (17)$$

$$Q^2_{T1g} \propto |X_c - X|^{2\beta} \quad (18)$$

The transition $Ia\bar{3}d \rightarrow I4_1/a$ induces the two strain components e^{elas} and e^{add}. For this reason we obtain two strain relations:

$$|X_c - X|^{2\beta} \propto e_{11}{}^{elas} = -2e_{33}{}^{elas} \quad (19)$$

$$|X_c - X|^{2\beta} \propto e^{add} \quad (20)$$

Also critical peak intensities behave according to the active representation, that of 222 being proportional to the square of the order parameter Q_{T1g} and, as deformation, proportional to composition

$$I_{222} = F(222)^2 \propto Q^2_{T1g} \propto |X_c - X|^{2\beta} \quad (21)$$

As shown above and in Fig. 3a, we obtain $\beta = 0.46(1)$ from the ferroelastic strain component (19), which is very close to the theoretical value of 0.5 for an ideal continuous phase transition of second order, and is also consistent with the behaviour of (222) intensities as a function of composition (Fig. 3b). Plotting I_{222} against $e_{11}{}^{elas}$ (Fig. 11) results in a straight line that passes through the zero point, as required by theory for a transition involving a single order parameter ($Q^2_{T1g} \propto I_{222} \propto e_{11}{}^{elas}$). The change in a_0' relative to the extrapolated a_0 implies that the volumes scale as Q^2_{T1g}. However, within the experimental error, we cannot derive the order parameter exponent for the volume strain e^{add} (20).

There exists a remote group-theoretical possibility that, instead of the single-step T_{1g} mechanism leading from $Ia\bar{3}d$ to $I4_1/a$ directly, the phase transition could proceed via an intermediate $I4_1/acd$ space group, by the

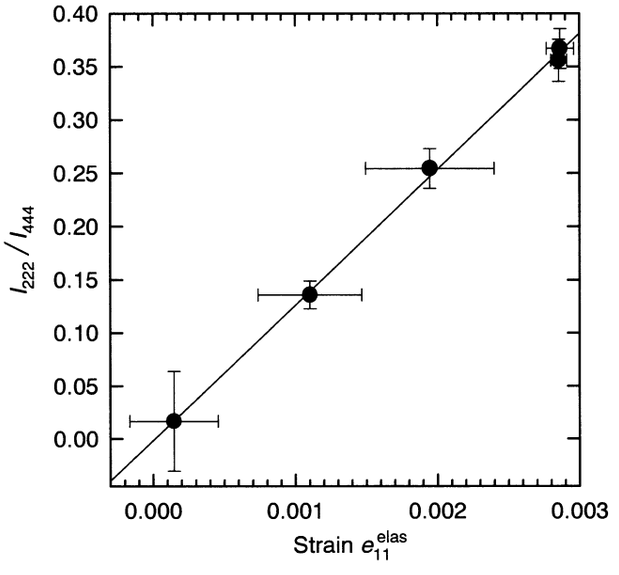

Fig. 11 Linear relationship between the normalized intensity of the (222) reflection (I_{222}/I_{444}) and the ferroelastic strain ($e_{11}{}^{elas}$) showing that $e_{11}{}^{elas} \propto I_{222}$

combination of a proper ferroelastic transition (E_g) and a ferrobielastic transition (A_{2g}) as in leucite (Palmer et al. 1990). On the basis of the observations and crystal chemical considerations, this path can be excluded because *i*) it would, in $I4_1/acd$, create two distinct dodecahedral sites but keep the disorder on the octahedral sites, *ii*) the order parameter exponent of the proper ferroelastic phase transition $\beta_{Eg}=2\beta_{T1g}$ would become unrealistically high ($\beta_{Eg}=0.92$ instead of falling into the range 1/3 to 1/2, Landau 1937a, b) and *iii*) due to coupling of two independent order parameters Q_{Eg} ($\propto e_{11}^{elas}$) and Q_{A2g} ($\propto I_{222}$), the I_{222} vs. e_{11}^{elas} relationship (Fig. 11) could not be linear nor pass through the zero point.

We conclude that the cubic to tetragonal phase transition in Al-poor majorite garnets proceeds via a single improper ferroelastic (T_{1g}) step from space group $Ia\bar{3}d$ to $I4_1/a$ by an ordering mechanism, that both the merohedral and pseudomerohedral twins in these garnets are produced during this same step, and that the phase transition is second order within experimental error.

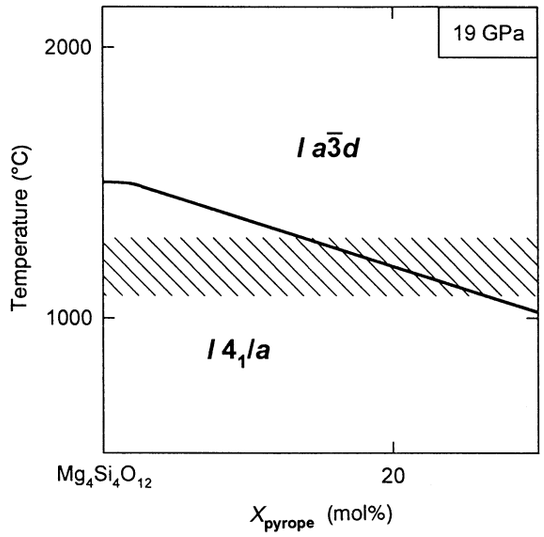

Fig. 12 Derived schematic isobaric *T-X* phase diagram for Al-poor majorites at 19 GPa. The *shaded area* represents the estimated cut-off temperature at which intracrystalline ordering processes are frozen in for the given quench rate

Derived isobaric *T-X* phase diagrams for garnets in the system $Mg_4Si_4O_{12}$-$Mg_3Al_2Si_3O_{12}$

The above observations combined with the conclusions of the Landau treatment may be combined in the form of a *T-X* phase diagram at 19 GPa. In doing so, we neglect the fact that the alumina-poor garnets of the system become unstable with respect to either $MgSiO_3$-ilmenite or β-Mg_2SiO_4+stishovite below about 1700 °C (Yusa et al. 1993) and only treat homogeneous (possibly metastable) equilibria between the garnet polymorphs.

For a second-order phase transition, no two-phase field of coexisting tetragonal and cubic garnet will exist, but the stability fields of the tetragonal and cubic garnets will be separated by a single curve, the shape of which is determined by the combination of the temperature- and composition-dependent terms of the polynomial expansion given above. Figure 12 presents the derived phase diagram. It was concluded above that all the garnets of the system grew at 2000 °C, 19 GPa in the stability field of the cubic phase. From the similarity in microtextures this argument probably also applies to the majorite end member synthesized at 17 GPa, 1800 °C by Angel et al. (1989). The phase transition to tetragonal symmetry in low-Al garnets therefore occurs at temperatures certainly below 2000 °C and most likely below 1800 °C. On the other hand, garnets with more than 20 mol% pyrope component are preserved with cubic symmetry. Because the phase transition to the $I4_1/a$ structure involves ordering on octahedral sites which requires diffusion, the compositional phase transition cannot represent the equilibrium boundary between cubic and tetragonal structures at room temperature but rather at an elevated temperature, where the intracrystalline order-disorder equilibrium is frozen in. We estimate this temperature to be at or above 1000 °C (shaded area in Fig. 12) from the following considerations. Brown and Navrotsky (1989) showed that intracrystalline Mg-Ti order in karrooite (pseudobrookite-type $MgTi_2O_5$) can only be quenched in at temperatures $\leq$1000 °C. This example is particularly relevant because it involves octahedral sites and the ordering of a divalent and a quadrivalent species, as in the majorites studied here. For the latter, the cut-off temperature might be somewhat higher than in karrooite because *i*) garnet has a particularly dense structure inhibiting diffusivities (Dowty 1980), *ii*) diffusion coefficients generally decrease with pressure, and *iii*) the quench in the multianvil press might have been faster than in the 1 bar experiments of Brown and Navrotsky (1989) for karrooite. This implies that the critical garnet composition (20 mole% pyrope) encountered in the experiments here is strictly valid only for the quench rate used (Seifert and Virgo 1974), which was equal in all our experiments. Only for these conditions of quench, the cut-off temperature is estimated to be slightly above 1000 °C (Fig. 12), and the corresponding critical concentration is 20 mole% pyrope. Slower quench rates will therefore shift the critical concentration to slightly higher pyrope concentrations. This interpretation is nicely confirmed by a recent study by Parise et al. (1996) who observed, on slow quench, a critical composition near 25 mole% pyrope.

According to these results, the cubic-tetragonal phase transition in garnets on the majorite-pyrope join, as shown in Fig. 12, occurs exclusively outside their stability field, i.e. it is a metastable phase transition. For instance, at 19 GPa and $\sim$1100 °C, the limiting composition of stable pyrope-majorite solid solutions is about 65 mole% pyrope (Gasparik 1992).

Volume, pressure effects and ordering mechanisms

It has been shown above that the tetragonal garnets have a larger volume than the (extrapolated) cubic ones (Fig. 2b) and that ordering of Mg and Si on octahedral sites increases the volume. This implies that an increase in pressure will stabilize the cubic (disordered) garnet structure. As the latter will probably have higher entropy than the ordered phase, the Clausius-Clapeyron slope of the phase transition in *P-T* space is expected to be negative.

The increase in volume during ordering combined with the ordering scheme as determined by Angel et al. (1989, see also Phillips et al. 1992) may give further clues about the phase transition itself. The garnet structure may be described as a closest packing of cylinders in ⟨111⟩ directions formed by connecting octahedral sites (Andersson and O'Keefe 1977, their Fig. 2). Orienting the tetragonal majorite structure parallel to [111], a central row of octahedra is then filled with alternating MgO_6 and SiO_6 octahedra but surrounded by six parallel octahedral cylinders which contain either MgO_6 or SiO_6 exclusively. MgO_6-bearing cylinders should have a longer unit repeat than the ordered $(Mg,Si)O_6$-bearing cylinders, whereas SiO_6-bearing cylinders would be shorter. The longer repeat unit will most likely determine the metrics of the unit cell, thus pointing to the cause for the larger volume of the ordered vs the disordered phases.

The necessary ordering step for the formation of the $I4_1/a$ phase also provides an explanation for the decrease in transition temperature with increasing Al content. The Al occupies the octahedral sites, blocking them and thus hindering Mg-Si diffusion and ordering, as seen from the nanometer size of the merohedral twins in the $Ma_{84}Py_{16}$ sample.

Applications to majoritic garnets in the Earth's mantle transition zone and in meteorites

We now return to the question of whether majorite-bearing garnets in the natural environment are expected to be cubic or tetragonal under formation conditions. Evidence for their composition (and, to a much lesser extent, for their symmetry) comes from three sources of information: (1) majorite-rich garnets in shocked meteorites, (2) high-pressure – high-temperature experiments on complex compositions similar to those expected in the transition zone and (3) inclusions of majorite-bearing garnets in diamonds believed to come from the transition zone (Haggerty and Sauter 1990; Moore et al. 1991). In comparing the chemistries of these garnets to those studied here in the system $Mg_4Si_4O_{12} - Mg_3Al_2Si_3O_{12}$, we use the silica content, expressed as number of Si atoms per 12 oxygens (per formula unit, pfu), as the prime parameter indicating the (maximum) proportion of a majorite end member component. In doing this we neglect the likely but largely unknown influence of other cations such as Fe^{2+}, Ti, Na, Ca and possibly Fe^{3+} on symmetry. Stabilization of the cubic structure has only been demonstrated for the $2Na^{VIII}+Si^{VI} \Psi 2Mg^{VIII}+Mg^{VI}$ substitution, which results in a $Na_2MgSi_5O_{12}$ end member (Hazen et al. 1994). Neglecting the latter substitution, the critical Si content for the cubic to tetragonal phase transition for our quenched majoritic garnets is then Si=3.8 pfu.

Majoritic garnets from shocked chondrites (e.g. Smith and Mason 1970; Price et al. 1979; Coleman 1977; Jeanloz 1981; McMillan et al. 1989; Langenhorst et al. 1995; Chen et al. 1996) range from 3.55 to 3.99 Si pfu. The highest contents of the majorite end member are found in low-Al garnets that transformed directly from enstatite, whereas the more Al-rich compositions, found in the matrix of shock veins, crystallized from a shock-induced melt (Chen et al. 1996). As fas as it is known, all of those majorite garnets have cubic symmetry. This is expected for those phases that have significant Al contents (Si=3.64 to 3.78, Smith and Mason 1970; Langenhorst et al. 1995; Chen et al. 1996), but rather surprising for the low-Al majorites with Si=3.91 to 4.01 (Coleman 1977; Price et al. 1979; Jeanloz 1981; Chen et al. 1996). One explanation could be that their relatively high [Fe]/([Fe]+[Mg]) ratios (0.20 to 0.27) stabilise the cubic structure (Kato 1986; Wang et al. 1993; their Fig. 6). Matsubara et al. (1990) as well as Ohtani et al. (1990) do not confirm this, but instead show that the c_{tet}/a_{tet} ratio of majorites is largely independent of [Fe]/([Fe]+[Mg]). An alternative explanation is that the apparent cubic symmetry of low-Al garnets is due to an extremely rapid quench from shock conditions such that the cut-off temperature for ordering is higher than that of the phase transition even in the most Si-rich garnets (cf. Fig. 12).

The amount of majorite component in the garnets of the Earth's transition zone will depend on pressure, temperature and bulk composition. For a natural garnet peridotite composition Takahashi and Ito (1987) showed that the Si contents of the majorite garnets increase from ca. 3.24 Si pfu at 13 GPa, 1650 °C (roughly corresponding to the 400 km discontinuity) to 3.69 Si pfu at 20 GPa, 1600 °C (slightly above the 660 km discontinuity). The same trend is seen in the data of Ohtani et al. (1995) in a primitive peridotite, with Si contents increasing from 3.27 Si pfu at 13.5 GPa, 1850 °C to 3.64 at 17.5 GPa, 1795 °C and in the data of Herzberg and Zhang (1996) on anhydrous peridotite KLB-1. At higher pressures in pyrolite compositions, on the other hand, Si contents in the garnets decrease from 3.58 at 23 GPa, 1500 °C to 3.41 at 25 GPa, 1500 °C (Irifune 1994). These findings are consistent with the observations by Irifune and Ringwood (1987, 1993) on a "pyrolite minus olivine" and MORB composition, respectively. In chondritic bulk compositions, values between 3.55 and 3.63 Si pfu have been reported at 16–20 GPa, 1900–2000 °C (Ohtani et al. 1989; Yurimoto and Ohtani 1992), and of 3.73 Si pfu at 26 GPa, 2050 °C by Agee (1990). At lower mantle pressures, garnet, if it exists, seems to be highly aluminous (O'Neill and Jeanloz 1994). Only Irifune and Ringwood (1987, 1993), Ohtani et al. (1995) and O'Neill and Jeanloz (1994) checked for the symmetry of the synthesized

garnets (range 3.18 to 3.63 Si pfu) and found them to be cubic after quench. In summary, garnets richest in the majorite component can be expected near the base of the transition zone and 3.73 Si pfu (corresponding to 73 mol% majorite end member) is the highest value reported for garnets in such experimental studies. For most parts of the transition zone, values between 3.3 and 3.6 Si pfu seem to be a reasonable estimate.

Moore et al. (1991) published analyses of majoritic garnets occurring as inclusions in diamonds and Haggerty and Sauter (1990) described garnet+clinopyroxene inclusions interpreted as exsolution products of a previous majoritic garnet. In both cases, a source in or near the transition zone was inferred. These garnets range in composition from 3.02 Si pfu (virtually majorite-free garnet) to 3.34, i.e. a maximum of 34 mol% majorite end member.

In summary, we conclude that garnets in the transition zone should have cubic symmetry rather than tetragonal symmetry because the pyrope content of such garnets is greater than the critical value of 20 mol% and temperatures in the transition zone are much higher than the transition temperature estimated for such compositions (cf. Fig. 12). This is in contrast to the conclusion made by Wang et al. (1993) that majorites in this region of the mantle must be tetragonal because their estimate of the transition temperature for end member majorite is far above temperatures expected in the transition zone. Hatch and Ghose (1989), using the interpretation of Angel et al. (1989), also concluded that majorite should be cubic in the transition zone. The transformation temperature for the end member majorite is not critically important because the natural garnets do not approach the end-member composition. The transition temperature that is relevant is that for majorites with 3.25 to 3.75 Si pfu. We have shown that for majorite with 3.8 Si pfu the transition temperature is approximately 1000 to 1300 °C at 19 GPa and decreases with increasing pyrope content (Fig. 12). The effect of additional components such as Fe^{3+} and Na is likely to further stabilise the cubic structure of majorite in the transition zone.

Possible effects of a cubic-tetragonal phase transition on the elasticity of transition zone garnets

Although transition zone garnets are too pyrope rich to have a tetragonal structure, their elastic properties may still be influenced by the phase transformation. Ferroelastic phase transitions as well as other phase transitions commonly result in a softening of elastic properties at temperatures well above and below the transition temperature (Poirier 1982; Salje 1990). The softening effect is generally greater on the low symmetry side of the transition, but can extend to temperatures much higher than the transition temperature (see examples in chapter 5 of Salje 1990). Softening of the Youngs modulus is very strong for the $Ia\bar{3}d \rightarrow I4_1/a$ transition in the $Ca_3Mn_2Ge_3O_{12}$ garnet (Fig. 13a; Kazey et al. 1982),

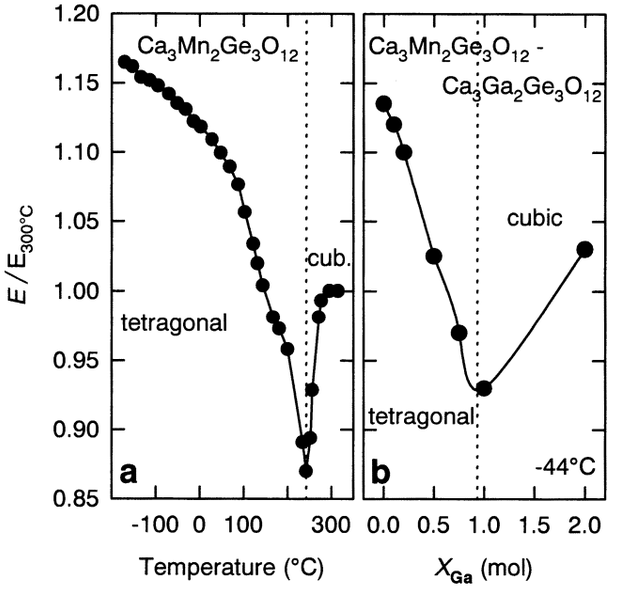

Fig. 13 a, b Influence of the cubic to tetragonal symmetry change on the Young's modulus in $Ca_3Mn_2Ge_3O_{12}$ garnet, **a** as a function of temperature and **b** as a function of composition in the garnet solid solution $Ca_3Mn_2Ge_3O_{12} - Ca_3Ga_2Ge_3O_{12}$. (After Kazey et al. 1982)

which suggests that such a softening effect could also play a role in majorite garnets within the transition zone. This effect will only be important in the mantle transition zone if softening is also a strong function of composition. Taking the data of Kazey et al. (1982) for the transition in the $Ca_3Mn_2Ge_3O_{12}$-$Ca_3Ga_2Ge_3O_{12}$ garnet system, we can construct a softening vs composition diagram (Fig. 13b). It is clear from Fig. 13b that softening is greater on the tetragonal side of the transition ($Ca_3Mn_2Ge_3O_{12}$ side) and that the softening effect may occur over a broad compositional range. Elastic constants determined for cubic phases along the majorite-pyrope join at room temperature (Bass and Kanzaki 1990; Yeganeh-Haeri et al. 1990; Hazen et al. 1994; Rigden et al. 1994) provide the only data for modelling the majorite contribution to seismic profiles in the transition zone. These data do not show a softening effect, possibly because they do not extend to high enough majorite contents or because they were measured at $\sim$1000 °C below the temperature where the transition is kinetically possible. Because elastic softening is common in ferroelastic transitions, it would be important to investigate this effect in majorite as a function of composition at high P and T. The seismic velocity within the transition zone is approximately 2% lower than modelled velocities based on elasticity data for a homogeneous mantle composition (Duffy and Anderson 1989; Jackson and Rigden 1997). Elastic softening of majorite garnets under transition zone conditions may provide a solution to this discrepancy and therefore must be investigated at high P and T if the seismic profiles of the transition zone are to be successfully modelled.

Acknowledgements We thank Ulrich Bismayer, Desmond McConnell, Simon Redfern, Ekhard Salje and particularly Ross Angel for helpful discussions of individual aspects of this paper. Constructive comments by an anonymous reviewer are appreciated. We thank R. Liebermann for providing a preprint of the Parise et al. (1996) manuscript. Andre Hogrefe synthesized the pyroxene used for $Mg_4Si_4O_{12}$ synthesis. Technical support by Dante Canil, Hubert Schulze and Herbert Küfner and financial support by Fonds der Chemischen Industrie to FS are gratefully acknowledged.

References

Agee CB (1990) A new look at differentiation of the Earth from melting experiments on the Allende meteorite. Nature 346: 834–837

Aizu K (1969) Possible species of "ferroelastic" crystals and of simultaneous ferroelectric and ferroelastic crystals. J Phys Soc Jap 27: 387–396

Akaogi M, Akimoto S (1977) Pyroxene-garnet solid solution equilibria in the system $Mg_4Si_4O_{12}$-$Mg_3Al_2Si_3O_{12}$ and $Fe_4Si_4O_{12}$-$Fe_3Al_2Si_3O_{12}$ at high pressures and temperatures. Phys Earth Planet Inter 15: 90–106

Andersson S, O'Keefe M (1977) Body-centred cubic cylinder packing and the garnet structure. Nature 267: 605–606

Angel RJ, Finger LW, Hazen RM, Kanzaki M, Weidner DJ, Liebermann RC, Veblen DR (1989) Structure and twinning of single-crystal $MgSiO_3$ garnet synthesized at 17 GPa and 1800 °C. Am Mineral 74: 509–512

Bass JD, Kanzaki M (1990) Elasticity of majorite-pyrope solid solution. Geophys Res Lett 17: 1989–1992

Brown NE, Navrotsky A (1989) Structural, thermodynamic and kinetic aspects of disordering in the pseudobrookite-type compound karrooite, $MgTi_2O_5$. Am Mineral 74: 902–912

Canil D (1994) Stability of clinopyroxene at pressure-temperature conditions of the transition region. Phys Earth Planet Inter 86: 25–34

Chen M, Sharp TG, El Goresy A, Wopenka B, Xie X (1996) The majorite-pyrope+magnesiowüstite assemblage: constraints on the history of shock veins in chondrites. Science 271: 1570–1573

Coleman C (1977) Ringwoodite and majorite in the Catherwood meteorite. Can Mineral 15: 97–101

Dowty E (1980) Crystal-chemical factors affecting the mobility of ions in minerals. Am Mineral 65: 174–182

Duffy TS, Anderson DL (1989) Seismic velocities in mantle minerals and the mineralogy of the upper mantle. J Geophys Res 94: 1895–1912

Gasparik T (1992) Melting experiments on the enstatite-pyrope join 80–152 kbar. J Geophys Res 97 B11: 15181–15188

Gnatchenko SL, Eremenko SV, Sofroneev NF, Kharchenko M, Devignes M, Feldmann P, LeGall A (1986) Spontaneous phase transitions and optical anisotropy in manganese germanium garnet ($Ca_3Mn_2Ge_3O_{12}$). Sov Phys JEPT 63: 102–109

Haggerty SE, Sauter V (1990) Ultradeep (greater than 300 kilometers) ultramafic mantle xenoliths. Science 248: 993–996

Hatch DM, Ghose S (1989) Symmetry analysis of the phase transition and twinning in $MgSiO_3$ garnet: implications to mantle mineralogy. Am Mineral 74: 1221–1224

Hazen RM, Downs RT, Conrad PG, Finger LW, Gasparik T (1994) Comparative compressibilities of majorite-type garnets. Phys Chem Minerals 21: 344–349

Heaney PJ, Veblen DR (1990) A high-temperature study of the low-high leucite phase transition using the transmission electron microscope. Am Mineral 75: 464–476

Heinemann S, Seifert F, Sharp TG, Rubie DC, Angel R (1994) Cubic-tetragonal symmetry change in garnets of the majorite-pyrope solid solution. Z Krist Supplement 8: 708

Herzberg C, Zhang JZ (1996) Melting experiments on anhydrous peridotite KLB-1 – compositions of magmas in the upper mantle and transition zone. J Geophys Res 101: 8271–8295

Irifune T (1994) Absence of an aluminous phase in the upper part of the Earth's lower mantle. Nature 370: 131–133

Irifune T, Ringwood AE (1987) Phase transformations in primitive MORB and pyrolite compositions to 25 GPa and some geophysical implications. In: Manghnani MH, Syono Y (eds) High pressure research in minerals physics. American Geophysical Union, Washington D.C., pp 231–242

Irifune T, Ringwood AE (1993) Phase transformations in subducted oceanic crust and buoyancy relationships at depths of 600–800 km in the mantle. Earth Planet Sci Lett 117: 101–110

Jackson I, Rigden SM (1997) Composition and temperature of the mantle: constraints from experimental studies of Earth materials. In: Jackson I (ed) The earth's mantle: composition, structure and evolution. Cambridge University Press (in press)

Janovec V (1974) A symmetry approach to domain structures. Ferroelectrics 12: 43–48

Jeanloz R (1981) Majorite: vibrational and compressional properties of a high-pressure phase. J Geophys Res 86: 6171–6179

Kato T (1986) Stability relation of (Mg,Fe)SiO_3 garnets, major constituents in the Earth's interior. Earth Planet Sci Lett 77: 399–408

Kazey ZA, Novak P, Soklov VI (1982) Cooperative Jahn-Teller effect in the garnets. Sov Phys JETP 56: 854–864

Krekels T, Van Tenedeloo G, Broddin D, Amelinckx, S, Tanner L, Mehbod M, Vanlathem E, Deltour R (1990) "Tweed" structure of Fe-doped $YBa_2Cu_3O_{7-\delta}$. Physica C 173: 361–376

Landau LD (1937a) Zur Theorie der Phasenumwandlung. I. Phys Zs Sowjetunion 11: 26–47

Landau LD (1937b) Zur Theorie der Phasenumwandlung. II. Phys Zs Sowjetunion 11: 545–555

Landau LD, Lifschitz EM (1980) Statistical Physics. Pergamon, New York

Langenhorst F, Joreau P, Doukhan JC (1995) Thermal and shock metamorphism of the Tenham meteorite: A TEM examination. Geochim Cosmochim Acta 59: 1835–1845

Matsubara R, Toraya H, Tanaka S, Sawamoto H (1990) Precision lattice-parameter determination of (Mg,Fe)SiO_3 tetragonal garnets. Science 247: 697–699

McMillan P, Akaogi M, Ohtani E, Williams Q, Niemann R, Sato R (1989) Cation disorder in garnets along the $Mg_3Al_2Si_3O_{12}$ – $Mg_4Si_4O_{12}$ join: an infrared, Raman and NMR study. Phys Chem Minerals 16: 428–435

Moore RO, Gurney JJ, Griffin WL, Shimizu N (1991) Ultra-high pressure garnet inclusions in Monastery diamonds: trace element abundance patterns and conditions of origin. Eur J Mineral 3: 213–230

Nord GL Jr (1992) Imaging transformation induced microstructures. In: Buseck PR (ed) Minerals and reactions at the atomic scale: transmission electron microscopy. Mineral Soc Am Rev Mineral 27: 455–505

Ohtani E, Kawabe I, Moriyama J, Nagata Y (1989) Partitioning of elements between majorite garnet and melt and implications for the petrogenesis of komatiite. Contr Mineral Petrol 103: 263–269

Ohtani E, Kagawa N, Fujino K (1990) Stability of majorite (Mg,Fe)SiO_3 at high pressures and 1800 °C. Earth Planet Sci Lett 102: 158–166

Ohtani E, Nagata Y, Suzuki A, Kato T (1995) Melting relations of peridotite and the density crossover in planetary mantles. Chem Geol 120: 207–221

O'Neill B, Jeanloz R (1994) $MgSiO_3$-$FeSiO_3$-Al_2O_3 in the Earth's lower mantle: Perovskite and garnet at 1200 km depth. J Geophys Res 99: 19901–19915

O'Neill HStC, McCammon CA, Canil DC, Rubie DC, Ross II CR, Seifert F (1993) Mössbauer spectroscopy of transition zone phases and determination of minimum Fe^{3+} content. Am Mineral 78: 456–460

Palmer DC, Putnis A, Salje EKH (1988) Twinning in tetragonal leucite. Phys Chem Minerals 16: 298–303

Palmer DC, Salje EKH, Schmahl WW (1989) Phase transitions in leucite: X-ray diffraction studies. Phys Chem Minerals 16: 714–719

Palmer DC, Bismayer U, Salje EKH (1990): Phase transitions in leucite: order parameter behaviour and the Landau potential deduced form Raman spectroscopy and birefringence studies. Phys Chem Minerals 17: 259–265

Parise JP, Wang Y, Gwanmesia GD, Zhang J, Sinelnikov Y, Chmielowski J, Weidner DJ, Liebermann RC (1996) The symmetry on the pyrope ($Mg_3Al_2Si_3O_{12}$) – majorite ($Mg_4Si_4O_{12}$) join. Geophys Res Lett 23: 3799–3802

Phillips BL, Howell DA, Kirkpatrick RJ, Gasparik T (1992) Investigation of cation order in $MgSiO_3$-rich garnet using ^{29}Si and ^{27}Al MAS NMR spectroscopy. Am Mineral 77: 704–712

Poirier JP (1982) On transformation plasticity. J Geophys Res 87: 6791–6797

Price GD, Putnis A, Agrell SO (1979): Electron petrography of shock-produced veins in the Tenham chondrite. Contrib Mineral Petrol 71: 211–218

Rigden SM, Gwanmesia GD, Liebermann RC (1994) Elastic wave velocities of a pyrope-majorite garnet to 3 GPa. Phys Earth Planet Int 86: 35–44

Ringwood AE (1991) Phase transformations and their bearing on the constitution and dynamics of the mantle.Geochim Cosmochim Acta 55: 2083–2110

Salje EKH (1990) Phase transformations in ferroelastic and coelastic crystals. Cambridge University Press, Cambridge

Salje EKH, Kuscholke B, Wruck B (1985) Domain wall formation in minerals: I. Theory of twin boundary shapes in Na-feldspar. Phys Chem Minerals 12: 132–140

Salje EKH, Bismayer U, Wruck B, Hensler J (1991): Influence of lattice imperfections on the transition temperature of structural phase transitions: the plateau effect. Phase Transitions 35: 61–74

Sapriel J (1975) Domain-wall orientations in ferroelastics. Phys Rev B 12: 5128–5140

Schmahl WW, Putnis A, Salje E, Freeman P, Graeme-Barber A, Jones R, Singh KK, Blunt J, Edwards PP, Loram J, Mirza K (1989) Twin formation and structural modulations in orthorhombic and tetragonal $YBa_2(Cu_{1-x}Co_x)_{7-\delta}$. Phil Mag Lett 60: 241–248

Seifert F, Virgo D (1974) Kinetics of the Fe^{2+}-Mg order-disorder reaction in anthophyllites: quantitative cooling rates. Science 188: 1107–1109

Shannon RD (1976) Revised effective ionic radii. Acta Crystallogr A32: 751–767

Smith JV, Mason B (1970) Pyroxene-garnet transformation in Coorara meteorite. Science 168: 832–833

Takahashi E, Ito E (1987) Mineralogy of mantle peridotite along a model geotherm up to 700 km depth. In: Manghnani MH, Syono Y (eds) High-pressure research in mineral physics. American Geophysical Union, Washington D.C., pp 427–437

Van Tendeloo G, Amelinckx S (1974) Group-theoretical considerations concerning domain formation in ordered alloys. Acta Crystallogr A30: 431– 440

Wang Y, Gasparik T, Liebermann RC (1993): Modulated microstructure in synthetic majorite. Am Mineral 78: 1165–1173

Warren MC, Ackland GJ (1996) Ab initio studies of structural instabilities in magnesium silicate perovskite. Phys Chem Minerals 23: 107–118

Weidner DJ (1986) Mantle models based on measured physical properties of minerals. In: Saxena SK (ed) Chemistry and physics of terrestrial planets. Springer-Verlag, Berlin Heidelberg New York, pp 251–274

Yamamoto N, Yagi K, Honjo G (1977a) Electron microscopic studies of ferroelectric and ferroelastic $Gd_2(MO_3)_3$. I. General features of ferroelectric domain wall, antiphase boundary and crystal defects. Phys Stat Sol (a) 41: 523–534

Yamamoto N, Yagi K, Honjo G (1977b) Electron microscopic studies of ferroelectric and ferroelastic $Gd_2(MO_3)_3$. II. Interactions between ferroelectric domain walls. Phys Stat Sol (a) 42: 257–265

Yeganeh-Haeri A, Weidner DJ (1990) Elastic properties of the pyrope – majorite solid solution series. Geophys Res Lett 17: 2453–2456

Yurimoto H, Ohtani E (1992) Element partitioning between majorite and liquid: a secondary ion mass spectrometric study. Geophys Res Lett 19: 17–20

Yusa H, Akaogi M, Ito E (1993) Calorimetric study of $MgSiO_3$ garnet and pyroxene: Heat capacities, transition enthalpies, and equilibrium phase relations in $MgSiO_3$ at high pressures and temperatures. J Geophys Res 98: 6453–6460